frontiers | Frontiers in Earth Science

ORIGINAL RESEARCH
published: 18 May 2022
doi: 10.3389/feart.2022.888012

Climate-Controlled Coastal Deposition of the Early Permian Liangshan Formation in Western South China

Ao Liu[1], *Jianghai Yang*[1,2]*, *Liang Cheng*[1] *and Juntong Ren*[1]

[1]School of Earth Sciences, China University of Geosciences, Wuhan, China, [2]State Key Laboratory of Biogeology and Environmental Geology, China University of Geosciences, Wuhan, China

During the late Paleozoic ice age, tropical coastal depositions have been widely linked to high-frequency sea-level variations, but their linkage with the associated climate change was not fully understood. In the early Permian, two deglaciations occurred in the late Sakmarian and late Artinskian, respectively. During the late Artinskian deglacial warming and transgression, coal-bearing siliciclastic successions of the Liangshan Formation were developed in South China. Three facies associations were recognized from the Liangshan Formation successions in western South China and ascribed to coastal alluvial plain, estuarine, and deltaic environments. Detailed analysis of sedimentology, paleosol morphology, and sandstone petrology suggest a relatively dry-to-wet climate shift and estuarine to deltaic facies transition in the lower Liangshan Formation. This climate shift and facies transition can be temporally correlated based on regional stratigraphic correlations, although precise age constraints are needed to test this correlation. The estuarine interval of the lowest Liangshan Formation signified a rapid transgression during the late Artinskian deglaciation and likely formed during a relatively arid climate with locally small fluvial systems, which provided limited sediment supply. The subsequent transition to and initiation of deltaic deposition was broadly associated with the inferred climate shift and could be primarily resulted from a climate wetting-induced great increase in sediment supply, irrespective of the deglacial sea-level rise.

Keywords: early Permian, coastal deposition, Liangshan Formation, climate change, western South China

OPEN ACCESS

Edited by:
Xiting Liu,
Ocean University of China, China

Reviewed by:
Xia Wang,
Chengdu University of Technology, China
Bo Chen,
Nanjing Institute of Geology and Paleontology (CAS), China

***Correspondence:**
Jianghai Yang
yangjh@cug.edu.cn

Specialty section:
This article was submitted to Marine Geoscience, a section of the journal Frontiers in Earth Science

Received: *02 March 2022*
Accepted: *14 April 2022*
Published: *18 May 2022*

Citation:
Liu A, Yang J, Cheng L and Ren J (2022) Climate-Controlled Coastal Deposition of the Early Permian Liangshan Formation in Western South China. Front. Earth Sci. 10:888012. doi: 10.3389/feart.2022.888012

INTRODUCTION

The late Paleozoic ice age (LPIA) is the longest icehouse climate period, with glaciations developed in the Gondwana continents and lasted more than 70 Myr from the Carboniferous to the Permian (Crowell, 1999; Isbell et al., 2003; Wopfner, 2013). This icehouse climate reached its acme glaciation in the earliest Permian and then gradually demised through the Permian before completely transferring into the Triassic greenhouse (Fielding et al., 2008; Montañez and Poulsen, 2013). There were well-developed distinctive, repetitive stratal stacking successions in the palaeotropical regions during the Pennsylvanian to early Permian (e.g., Wanless and Shepard, 1936; Montañez and Poulsen, 2013; Fielding, 2021). Detailed studies on these tropical cyclical strata revealed high-frequency eustatic sea-level variations driven by the

glacial–interglacial cycles in the high latitudes (Wanless and Shepard, 1936; Ross and Ross, 1985; Heckel, 1986; Smith and Read, 2000; Rygel et al., 2008; Belt et al., 2011; Fielding and Frank, 2015, 2020). These cyclic sequences record changes in paleosols and palaeofloras, reflecting associated climate fluctuations in tropical regions (Tandon and Gibling, 1994; Miller et al., 1996; Cecil et al., 2003; Olszewski and Patzkowsky, 2003; Falcon-Lang, 2004; Dolby et al., 2011; Eros et al., 2012; Rosenau et al., 2013).

The control of sea-level variations on the LPIA coastal sedimentation has been widely documented (e.g., Wanless and Shepard, 1936; Fielding, 2021). However, the role played by climate on the sedimentary patterns has not been well distinguished from those of sea-level fluctuations during the LPIA (Fieldman et al., 2005), although long-term, intermediate, and short-term dry-to-wet climate shifts have been increasingly recognized (e.g., Miller et al., 1996; Cecil et al., 2003; Olszewski and Patzkowsky, 2003; Falcon-Lang, 2004; Tabor and Poulsen, 2008; Eros et al., 2012). Cecil et al. (2003) highlighted the potential primary control of short-term climate changes on Pennsylvanian–early Permian cyclic lithostratigraphy (e.g., Cecil, 1990; Miller et al., 1996). Fieldman et al. (2005) advocated a dominant control of intermediate climate changes on the fluvial sediment supply and sequence architecture of the Pennsylvanian glacio-eustatic sequences based on pedogenic fabrics and low-stand depositions. All these studies focused on the Permo-Carboniferous records in tropical Pangea but with few or no data coming from tropical Tethys regions where the continuous marine successions are well developed during the Permian icehouse-to-greenhouse transition (e.g., Liu and Xu, 1994; Wang et al., 2013; Shen et al., 2019).

During the late early Permian main deglaciation (e.g., Fielding et al., 2008), coal-bearing siliciclastic depositions were widely developed in South China, named as the Liangshan Formation, in association with the late Artinskian transgression (Wang et al., 2013; Shen et al., 2019). To further understand the importance of climate effects relative to that of sea-level changes on tropical coastal sedimentation, we here conducted a detailed study on the Liangshan Formation in western South China in terms of sedimentology, mineralogy, and geochemistry. This study reveals a significant control of the dry-to-wet climate shift on the coastal strata architecture during the deglacial sea-level rise.

GEOLOGICAL SETTINGS AND STUDIED SECTIONS

The South China Block is bounded by the Qinling–Dabie–Sulu orogenic belt to the north (Meng, 2017) and by the Jinshajiang–Ailaoshan orogenic belt to the west (Wu, 1998; Zhang et al., 2013). It was formed by the Proterozoic collisional assembly between the Yangtze and Cathaysia blocks along the Jiangnan orogenic belt (Li et al., 2002; Wang and Li, 2003; Li et al., 2009; Shu et al., 2011). In South China, there were mainly marine carbonate and shale sequences through the late Neoproterozoic to early Paleozoic, and a regional unconformity separates the early Paleozoic limestones and shales from the overlying late Paleozoic marine carbonate-dominated successions (Liu and Xu, 1994). During the late Paleozoic, South China was located in tropical regions and achieved relatively continuous sedimentary successions in stable cratonic settings (Liu and Xu, 1994; Wang et al., 2018). For the Pennsylvanian–early Permian interval, sequence stratigraphy, lithofacies and carbon–oxygen isotopic analysis exhibited high-frequency sea-level fluctuations and climate changes related to the late Paleozoic glaciations (Buggisch et al., 2011; Wang et al., 2013; Liu et al., 2017; Huang et al., 2018). In South China, the late Pennsylvanian–early Permian strata are mainly composed of carbonates with abundant benthic faunas, including the Maping Formation in the western part and the Chuanshan Formation in the eastern part (e.g., Shen et al., 2019). A major seal-level fall occurred in the early Permian (possibly in the Sakmarian) and produced an extensive sedimentary hiatus through South China ((Liu and Xu, 1994; Wang et al., 2013; Shen et al., 2019). Subsequently, a coal-bearing siliciclastic sedimentary sequence of the Liangshan Formation was developed, especially in the surrounding areas of paleo-uplifts, and represents the basal part of the Yangsingian series of South China (Shen et al., 2019). It grades upward into the thick Kungurian limestones of the Chihsia Formation, the most widely distributed carbonate deposits in South China (Liu and Xu, 1994).

The Liangshan Formation is mainly composed of bauxites, massive mudrocks, quartzose sandstones, shales, and coal measures with or without a limestone interbed (Zhao and Huang, 1931; Jin and Fang, 1985). Relative to the abundant marine fossils in the carbonates of Chihsia and Maping formations, the Liangshan Formation is characterized by containing terrestrial sporo-pollens and plant fragments (e.g., Jin and Fang, 1985; Shi et al., 2014). Brachiopods are the most abundant marine fauna in the Liangshan Formation (Lv, 1982; Jin and Fang, 1985; Campi and Shi, 2007). The brachiopod assemblages are of the Artinskian in age based on their associated conodonts and thus provide an age constraint for the Liangshan Formation (Campi and Shi, 2007; Shen et al., 2019).

We carefully logged and sampled the successions of the Liangshan Formation from four sections in Weining and Pingtang regions in Guizhou province of western South China (**Figures 1**, **2**). The Xiuhe section is located in the northeast of Weining city (**Figure 1B**) and contains a siliciclastic succession of the Liangshan Formation with a thickness of ~85 m (**Figure 2A**). The Caohai section is located southwest of Weining city (**Figure 1B**) and contains a ~26-m-thick succession of the Liangshan Formation (**Figure 2B**). The Houpo section is located in the south of Pingtang city (**Figure 1C**) and has a ~25-m-thick succession of the Liangshan Formation (**Figure 2C**). The Mapojiao section is located in the east of Pingtang city (**Figure 1C**) and contains a coal-bearing succession of the Liangshan Formation of about 21 m in thickness (**Figure 2D**). The measured successions of the Liangshan Formation were all formed in an overall coastal marine environment (**Figure 1A**; Liu and Xu, 1994).

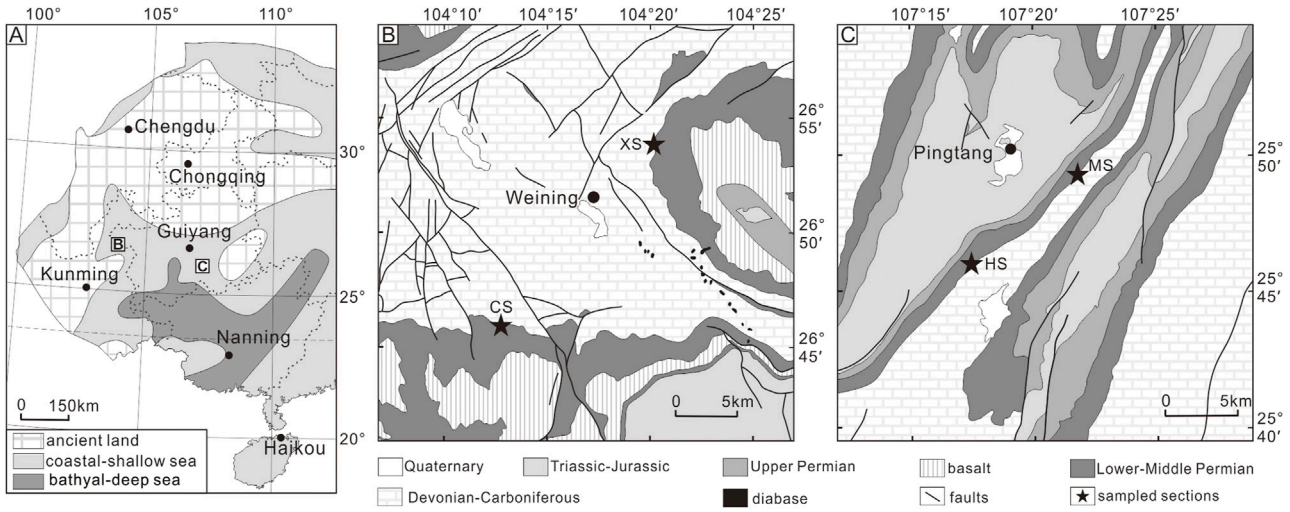

FIGURE 1 | Locations of the studied sections (XS: Xiuhe section, CS: Caohai section, HS, Houpo section, and MS: Mapojiao section) in the paleogeographic reconstruction for the deposition of early Permian Liangshan Formation in western South China (**A**, revised from Liu and Xu, 1994) and geologic maps in Weining and Pingtang regions (**B,C**, after GZBGMR, 1987).

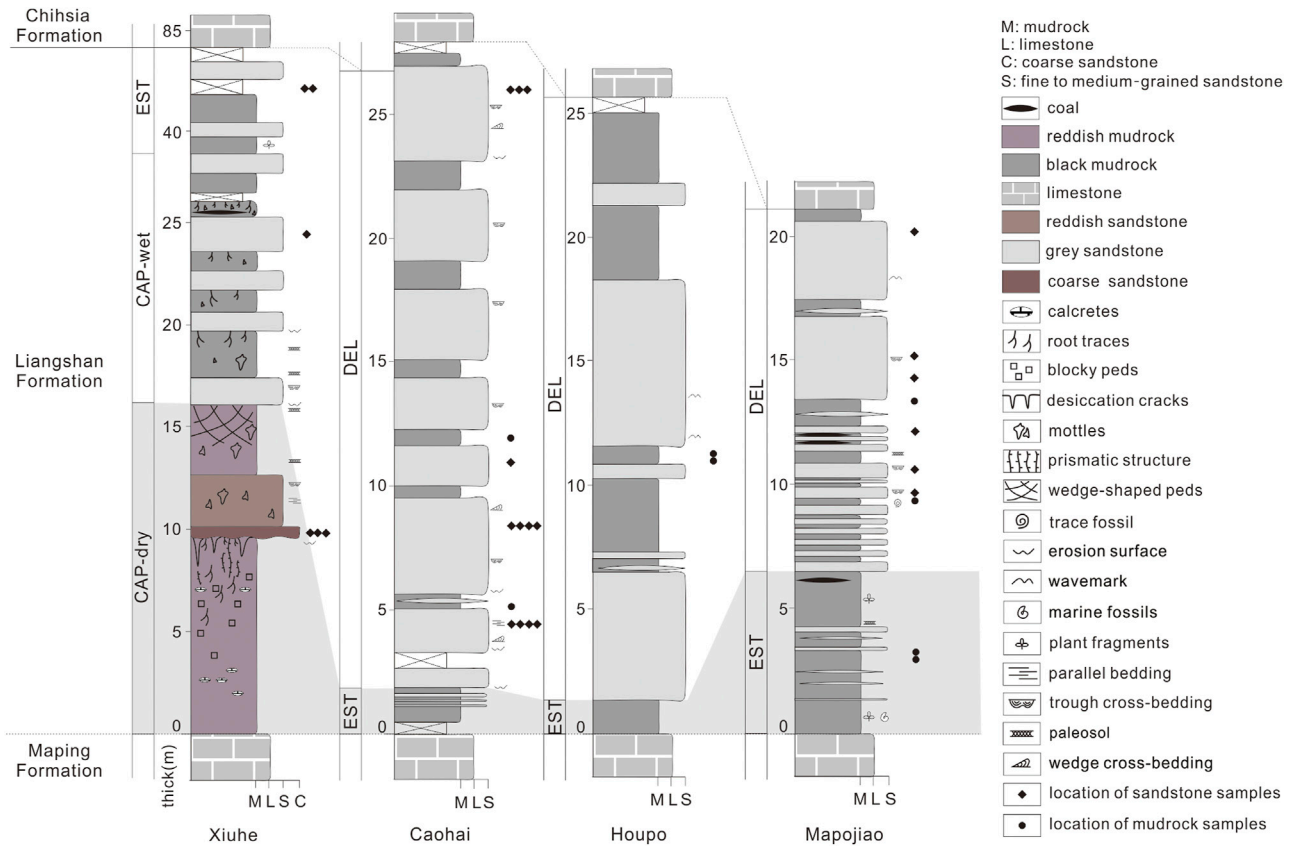

FIGURE 2 | Lithological columns of the logged successions from the top Maping through Liangshan to the basal Chihsia formations in the Xiuhe, Caohai, Houpo, and Mapojiao sections, showing the sedimentary structures of the strata, and stratigraphic positions of each sample analyzed during this study.

FIGURE 3 | Outcrop photographs of the Liangshan Formation in the Xiuhe section and the facies interpretations. **(A)** Unconformable contact (red dotted line) of the Liangshan Formation between the underlying Maping Formation (Hammer of ~30 cm, circled, for scale). **(B)** CAP facies associations at the lower Liangshan Formation, showing reddish mudrocks of the coastal floodplain, erosionally based sandstone bodies of the coastal plain channel, mottled mudrocks, and dark gray mudrocks. A remarkable color change from purplish red to dark gray was noted. **(C)** Close-up view of the blocky to prismatic ped structures, plant root traces, and calcareous nodules of reddish mudrocks. **(D)** Close-up view of the reddish coarse-grained sandstone bed of the coastal plain channel, showing fining upward trend. **(E)** Mottled mudrocks of coastal floodplain in arid climate covered by sandstones of the coastal plain channel and interbedded black mudrocks and sandstones of coastal floodplain in a more humid climate (Hammer of ~30 cm, circled, for scale). **(F)** EST facies associations above the coastal plain mudrocks, and sandstones. The mudrocks, sandstones, and carbonaceous shales of estuarine flat, tidal rhythmite, and estuarine mire are interbedded, and some intervals preserved estuarine channel sandstones.

SAMPLES AND ANALYTICAL METHODS

Sampling was conducted at intervals with good exposure and little alterations by present-day weathering. So, our sampling was not even through the logged successions, especially for the Houpo section where modern weathering is heavy. A total of 22 samples were collected from the Liangshan Formation, including three sandstone samples from the Xiuhe section, four sandstone samples and two mudrock samples from the Caohai section, and two mudrock samples from the Houpo section, and six sandstone and five mudrock samples from the Mapojiao section.

The sandstone samples were thin-sectioned and observed under a microscope. Their modal composition was determined by Gazzi–Dickinson point-counting method (Dickinson, 1970; Ingersoll et al., 1984). Detrital modes were characterized by the types and proportions of framework grains such as quartz and feldspar grains and lithic fragments (Dickinson, 1970). The mudrock samples were analyzed using X-ray diffraction (XRD) for mineralogical compositions and X-ray fluorescence (XRF) for major element contents. Mineralogical analyses by X-ray diffraction were performed with a PANalytical X'Pert Pro model instrument at the State Key Laboratory of Geological Process and Mineral Resources (GPMR), China University of Geosciences (Wuhan). The analytical error reported is 5% for clay minerals and 2% for non-clay minerals. The major elements were measured using a PANalytical Axios X-ray fluorescence spectrometer at ALS Chemex (Guangzhou, China). The analytical uncertainty is 5% for LOI (loss on ignition) and 2% for SiO_2, Al_2O_3, CaO, Fe_2O_3T, Na_2O, K_2O, MgO, MnO, and P_2O_5. The determination limit is 0.01% for the major elements.

SEDIMENTOLOGY AND FACIES INTERPRETATIONS FOR THE SAMPLED SUCCESSIONS

Three facies associations were recognized, following Fielding and Frank (2015), based on the relative abundances of mudrocks and sandstones, sedimentary structures, thicknesses of sandstone bodies and their vertical grain-size trends, and pedogenic characters. These are attributed to coastal alluvial plain (CAP), estuarine (EST), and deltaic (DEL) environments. The lithofacies and interpreted facies are briefly outlined in the following.

Coastal Alluvial Plain Facies Association

The CAP facies association comprised three facies: coastal plain channel, coastal plain floodplain, and coastal mire. These facies were recognized in the lower part of the Xiuhe section.

The coastal plain channel comprised erosionally based, fine- to coarse-grained sandstones (**Figures 3B,D,E**). Two sandstone beds were observed from the lower Liangshan Formation in Xiuhe section. The lower one was reddish in color with a thickness of about 2.5 m and showed fining upward trends from the basal coarse-grained sandstones to medium-grained sandstones at the top. Its bottom contained angular mudrock gravels, which tend to be diminished to the southwest, and had an erosional contact with the underlying red mudrocks. Parallel bedding, horizontal laminations, and cross-stratifications were observed. The upper one was medium- to fine-grained quartzose sandstone of about 1 m thickness. It had a distinct undulate erosional base. There developed pervasively trough cross-bedding and minor parallel bedding. This lithofacies was interpreted as the product of coarse-grained deposition in river channels in a coastal lowland plain. Considering their thickness, these sandstones might not represent major distributary channels. The lower coarse-grained sandstones might form in a weakly confined channel related to abrupt floods, and the upper sandstones likely represented a crevasse channel linked to a major tributary channel (e.g., Fielding, 2021).

The coastal plain floodplain consisted of massive mudrock and interbedded mudrocks and sandstones. The variety of colors of mudrocks in these lithofacies was noted. Mudrocks at the bottom with up to 10 m thickness displayed strong reddening and were characterized by intense pedogenesis. There developed obvious blocky to prismatic ped structures, calcareous nodules, vertical cracks filled with pale gray sandstones, and extensive disruption by *in situ* plant roots. The second mudrock unit in the Xiuhe section was dominated by pale red colors with drab gray mottling grading upward to the pale gray horizon at the top. Vertical structures and large-scale slickensides developed in these mottled mudrocks with carbonate nodules present in the lower part. Further upward, there occurred gray mudrock beds of about 0.5 m thickness, which were interbedded with the overlying medium-bedded, fine-grained sandstones. They show blocky ped structures and mottling in the lower part. There was no evidence of any grain-size trends, and tidal or storm surges were observed in this lithofacies. The sandstone layers were only about 0.1–0.4 m thick and were somewhat lenticular (**Figure 3B**). Mud-graded sediments probably fell from suspensions derived from overbank flows in nearby channels and were subsequently altered by pedogenic processes. Tabular sandstones were likely delivered in gentle currents probably from the same source and represented distal crevasse splay sheet-lite deposits.

The coastal mire comprised beds of carbonaceous shale and impure coal of <0.5 m thickness, and abundant carbonized plant fragments can be observed in coal. This facies was interpreted as the deposition of the coastal mire that occupied floodplain surfaces once sediment had filled open standing water areas. The mire was obviously short-lived and immature according to the thin and impure nature of these beds (Fielding and Frank, 2015).

Estuarine Facies Association

The EST Facies Association comprised five facies: estuarine channel, estuarine bay fill, estuarine flat, tidal rhythmite, and estuarine mire. These facies were recognized in the upper Xiuhe section and the basal parts of the other three sections. In these intervals, the estuarine lithofacies were closely associated and can be distinguished from the underlying coastal alluvial plain or overlying deltaic depositions.

The estuarine channel consisted of erosionally based sandstone bodies of up to <2 m thickness (**Figure 4A**). These bodies somewhat resembled the CAP channel bodies but were thinner bedded with much finer, better sorted grains. They commonly had siltstone partings and tough cross-bedding sets. This lithofacies was interpreted as the product of the estuarine channel, within the lower reaches of the fluvial–tidal transition zone (Martinius and Gowland, 2011; Fielding and Frank, 2015).

The estuarine bay fill comprised a coarsening upward mudrock-dominated succession, with a thickness <1 m, passing from laminated mudrocks upward to fine-grained sandstones (**Figure 4A**). The coarsening upward nature suggested the filling of standing water by a prograding clastic system. This lithofacies was interpreted as a record filling shallow water estuarine bays. The estuarine flat comprised interlaminated and interbedded mudrocks and fine-grained sandstones of up to 3 m thickness, associated with other EST lithofacies (**Figures 3F**, **4A**,E). The mudrocks of this facies displayed dark gray to black color. There was no evidence of channel forms observed for the sandstone beds, which may have scour surfaces. It suggested a formation in relatively flat-lying surfaces at times exposed and others submerged. This lithofacies was interpreted as a product of estuarine flats ranging from subtidal to supratidal, where a relatively flat-lying surface was intermittently exposed or drown (Fielding and Frank, 2015).

The tidal rhythmite comprised rhythmically laminated, alternating mudrock and very-fine to fine-grained sandstone of up to 2 m thickness (**Figures 3F**, **4E**). The interlamination-signified rhythmic character made it the most distinctive facies. Abundant plant fragments and marine fossils (mainly brachiopods) were observed in mudrocks. This lithofacies was very similar to the so-called "tidal rhythmites" documented from modern and ancient tidal settings (Nio and Yang, 1991; Fielding and Frank, 2015). Therefore, it was interpreted as a subtidal to intertidal deposition dominated by tidal dynamics. Changes in current strength and direction were associated with the diurnal or

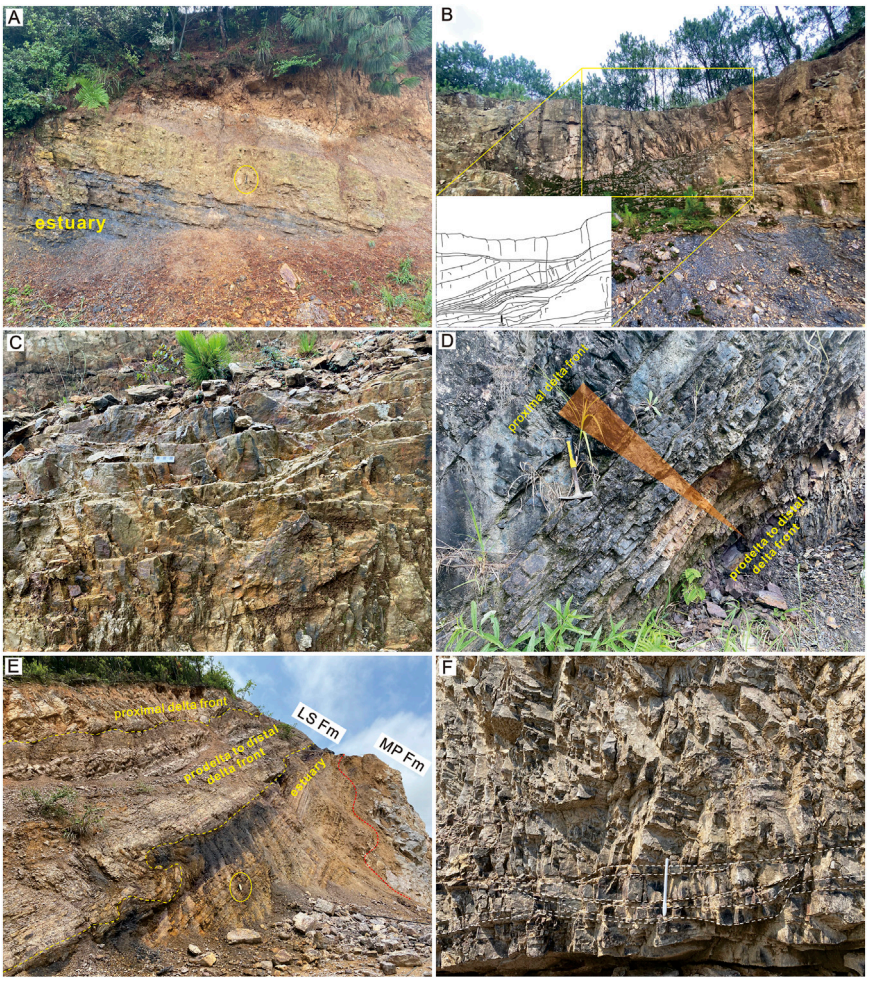

FIGURE 4 | Outcrop photographs of the Liangshan Formation in the Caohai, Houpo, and Mapojiao sections and the facies interpretations. **(A)** EST facies association at the basal part of Caohai succession, showing a coarsening upward sequence from estuarine bay mudrocks and sandstones to cross-laminated sandstones of the estuarine channel (Pen of 15 cm for scale). **(B)** Delta distributary channel sandstones in the Caohai section showing lateral accretion macroform overlying on planar bedded fine-grained quartzose sandstones of proximal delta front and mudrocks and siltstones of prodelta to distal delta front. **(C)** Close-up view of trough cross-stratified sandstones of delta distributary channel in the Caohai section. **(D)** Typical coarsening upward sequence of delta progradation in the Houpo section. **(E)** DEL and EST facies associations at the lower parts of the Mapojiao section. The distinctive interlamination mudrock and sandstone of tidal rhythmite facies are overlain by interbedded mudrocks and sandstones of prodelta to distal front facies (notebook of ~20 cm, circled, for scale). **(F)** Close-up view of cross-stratified fine-grained sandstones of proximal delta front and delta distributary channel facies in the Mapojiao section.

semidiurnal tide. The estuarine mire comprised carbonaceous shales and impure coal beds of about 1 m thickness (**Figures 3F**, **4E**). Abundant plant fragments were present. This lithofacies was interpreted as a product of estuarine mire, forming within estuarine basins.

Deltaic Facies Association

The DEL Facies Association comprised four facies of prodelta to distal delta front, proximal delta front, distributary channel, and delta plain mire. These facies were mainly observed in Caohai, Houpo, and Mapojiao sections.

The prodelta to distal delta front facies comprised laminated mudrocks and thinly interbedded mudrocks and fine-grained sandstone (**Figures 4B,D,E**). Sandstones were generally thinly bedded and lenticular. Bioturbations were noted in some mudrocks and are generally sporadic though locally abundant. Current and wave-generated sedimentary structures were noted in some sandstone bodies in Mapojiao section. This lithofacies was interpreted as having formed on the distal delta front and the prodelta environments, at or under a fair weather wave base. The prodelta to distal delta front facies showed coarsening upward trends grading upward into the proximal delta front sandstone facies and formed as the initial phase of delta progradational cycles.

The proximal delta front comprised typical coarsening upward bodies of sharp fine-grained sandstones in a <5m-thick succession. They were overlying prodelta to distal delta front facies (**Figures 4B,D,E**). The currently generated sedimentary structures dominated with a subordinate component of combined flow and wave-generated structures. There was

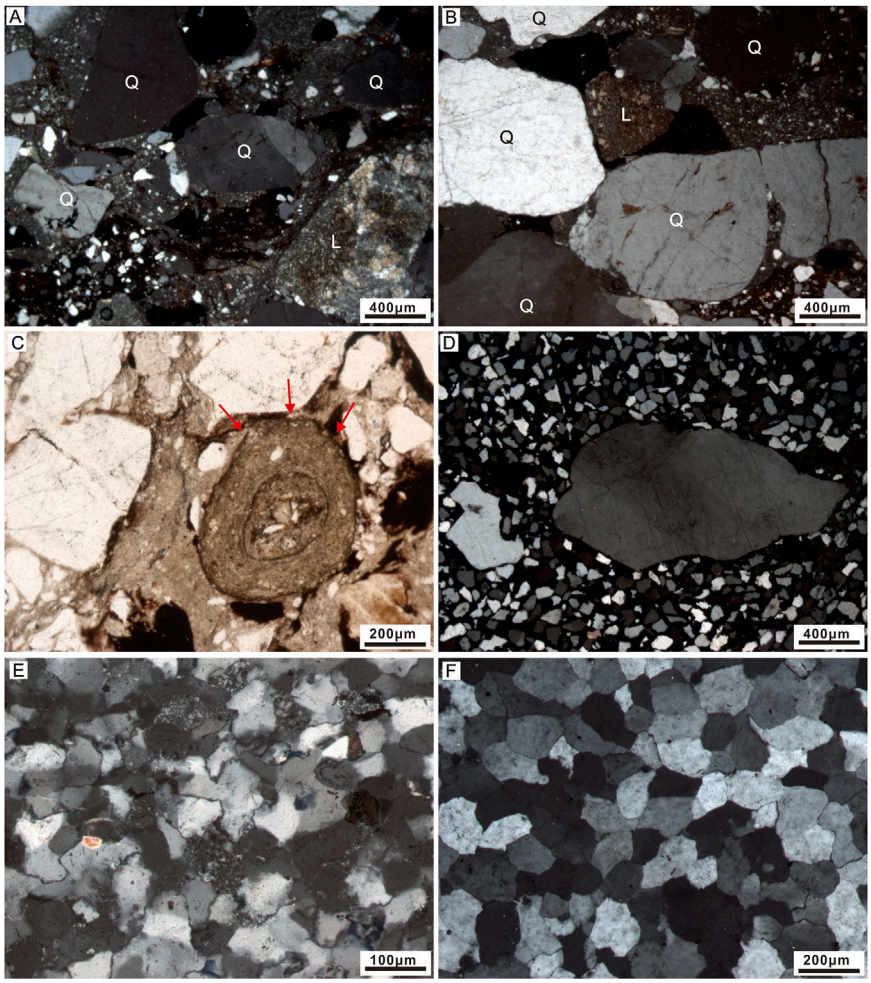

FIGURE 5 | Micrographs of sandstone samples from the Liangshan Formation. **(A,B)** Photomicrograph (cross-polarized light) of coarse-grained coastal plain channel sandstones from lower Xiuhe section, presenting high contents of silt-grained matrix, generally matrix-supported texture, and poorly sorted subangular to subrounded quartz grains (Q) and sedimentary lithic fragments (L, carbonate, mudrock, and siltstone) as framework components. **(C)** Photomicrograph (plane-polarized light) of coarse-grained coastal plain sandstones from Xiuhe section, showing a specific ooid-like lithic fragment with different-colored concentric laminae (arrowed). **(D)** Photomicrograph (cross-polarized light) of fine-grained coastal plain channel sandstones in lower Xiuhe section, showing well-sorted, subangular to subrounded quartz grains and outsized quartz grains, which range from coarse-grained sand to granules in size. **(E)** Photomicrograph (cross-polarized light) of fine-grained deltaic sandstones from the upper Caohai section. **(F)** Photomicrograph (cross-polarized light) of the fine-grained deltaic sandstones in the middle Mapojiao section. The deltaic sandstones are dominated by generally well-sorted, subrounded quartz grains, which are sometimes coalesced together by diagenesis.

considerable lateral facies variability with erosionally based channel bodies inset into this lithofacies in places (**Figure 4B**). The distributary channel consisted of erosionally based, fine-grained sandstone bodies. They commonly preserved tough cross-stratigraphy and wedge-shaped geometry with lateral accretion macroform cross-sets (**Figure 4B**). Coarsening upward sequences were noted in some bodies. Most part of cross-stratigraphy showed unimodal paleocurrents directed southwestward, and wave marks were observed on some sandstone body's surface. This facies was interpreted as the deposits of the delta distributary channel, dominated by fluvial currents with little wave influences. The river dispersed sediments southwestward to the coastal settings. The delta plain mire consisted of carbonaceous shale and impure coal beds of up to ~1 m thickness in Mapojiao section. This facies was associated with distributary channel sandstones and interpreted to record the peat deposition on the filled interdistributaries of the delta plain (Fielding and Frank, 2015).

SANDSTONE COMPONENTS AND MUDROCK MINERALOGY AND GEOCHEMISTRY

Coarse sandstone samples from the lower channel sandstones of the coastal alluvial plain in the lower Xiuhe section were rich in matrix (22.4–29.5%) and contained framework components of monocrystalline quartz (Q) grains (43.1–55.7%) and lithic fragments (L, 21.9–27.4%). They were generally matrix-supported in texture with quartz granules, and mud drapes

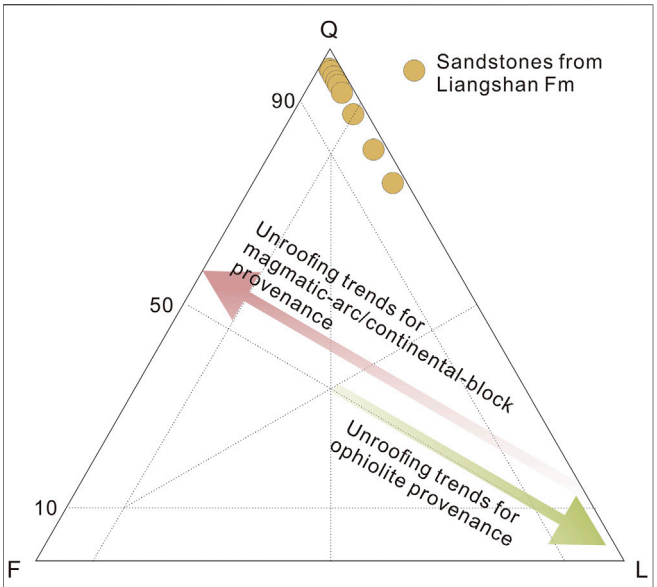

FIGURE 6 | Q-F-L (quartz–feldspar–lithic fragment) petrographic classification (Dickinson, 1970; Garzanti, 2016, 2019) of the sandstone samples from the Liangshan Formation, noting the coastal plain coarse sandstones with more lithic fragments.

occasionally observed and quartz grains were subangular to subrounded in shape. The lithic fragments were dominant of sedimentary origin with a few of metamorphic origin (quartz schist, 0–4.9%), including cherts (2.8–5.7%), mudrock (7.8–10.6%), and siltstone/very fine sandstone (7.7–12.4%) (**Supplementary Table S1**). Specific components observed, though in a very low concentration, were altered limestone fragments and ooid-like concretions with concentric laminae distinguished by different coloration (**Figure 5**). The upper alluvial plain channel sandstones were primarily composed of subangular to subrounded quartz grains. They were generally well sorted, but outsized quartz grains were occasionally present (**Figure 5**). The sampled deltaic sandstones were fine- to medium-grained in size and show grain-supported structure. Their framework components were dominated by quartz grains (>95%; **Figure 5**) with a few cherty fragments. The quartz grains were subrounded in shape and had a quite homogeneous grain size. Also there were stable accessory mineral grains like zircon and rutile. For both the alluvial channel and deltaic sandstones, there were no feldspar (F) grains observed. According to the Q-F-L petrographic classification of Garzanti (2019), lower alluvial channel sandstone samples were litho-quartzose sandstones, and upper alluvial plain channel and deltaic sandstones were quartzose sandstones (**Figure 6**).

XRD analysis shows that the mudrock samples primarily consisted of clay minerals and quartz grains (13–66% and 33–86%) with very few titanium bearing accessory minerals like anatase (**Figures 7A,B**; **Supplementary Table S2**). No feldspars were detected in the samples. Illite and kaolinite dominated the detected clay minerals and have a broadly negative correlation (r^2 = 0.32). The analyzed mudrock samples exhibited high and variable contents in SiO_2 (51.84–75.72%) and Al_2O_3 (12.56–28.10%), and very low contents in CaO and Na_2O (0.01–0.08% and 0.06–0.18%, respectively) (**Supplementary Table S3**). Relative to CaO and Na_2O, K_2O had a high content of 2.35–5.84%, with K_2O/Na_2O ratios of 16.8–53.1 much higher than those of the post-Archean average shale (3.08, Taylor and McLennan, 1985). The contents of Fe_2O_3, MgO, and TiO_2 were in the ranges of 1.39–6.03%, 0.65–1.48%, and 0.88–1.54%, respectively. The two mudrock samples from the estuarine facies had Al_2O_3/TiO_2 ratios of 24.1–26.5 higher than the corresponding ratios (12.2–18.2) of samples from the overlying deltaic facies (**Figure 7C**).

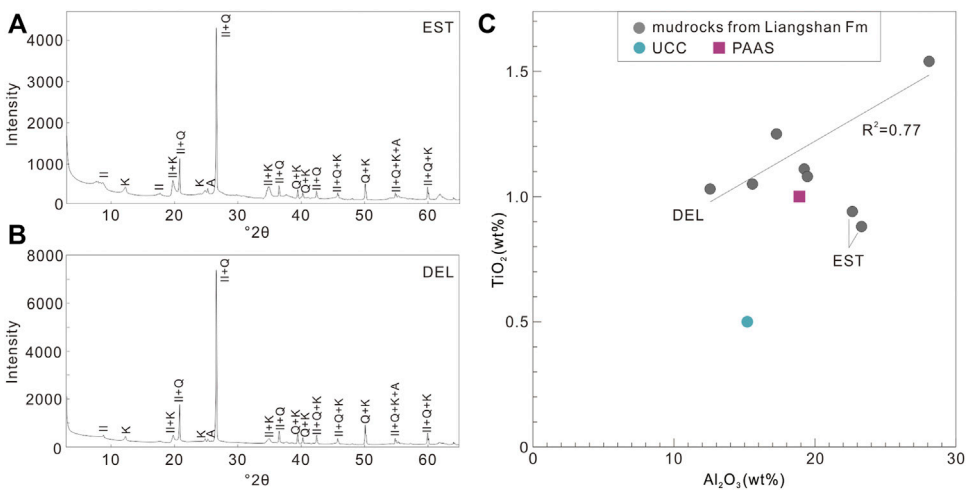

FIGURE 7 | XRD spectra of mudrock samples of the Liangshan Formation from **(A)** estuarine and **(B)** deltaic environments. **(C)** Al_2O_3-TiO_2 cross-plot for mudrock samples of the Liangshan Formation. Noting the positive correlation (R^2 = 0.77) of Al_2O_3 and TiO_2 for the deltaic mudrock samples. Data for PAAS (post-Archean average Australian shale) and UCC (upper continental crust) from Taylor and McLennan (1985) are also shown for comparison. Abbreviations: Il, illite; K, kaolinite; Q, quartz; A, anatase.

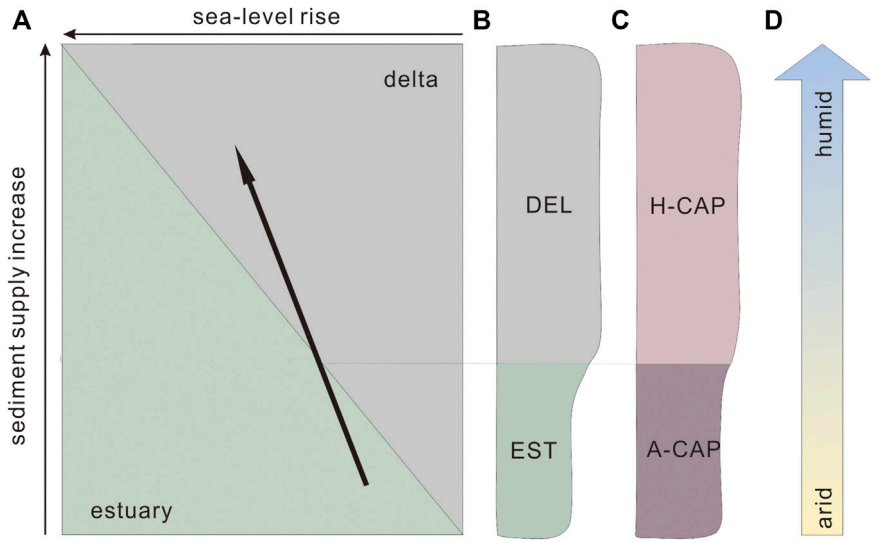

FIGURE 8 | Evolution and interpretation of the estuarine to deltaic facies transition in the lower Liangshan Formation. **(A)** Estuary to delta evolution model revised from Boyd et al. (1992), and the black arrow indicates the inferred estuarine to deltaic facies transition in the lower Liangshan Formation. **(B)** Sedimentary facies architecture of the lower Liangshan Formation based on the Caohai, Houpo, and Mapojiao successions. **(C)** Sedimentary facies architecture of the lower Liangshan Formation based on the Xiuhe succession. **(D)** Assumed relatively arid-to-humid climate shift recorded in the lower Liangshan Formation of the Xiuhe section.

DISCUSSIONS

Climate Shift in the Lower Liangshan Formation

There were distinct stratigraphic trends in pedogenic features, sandstone petrography, and lithofacies through the coastal alluvial plain intervals in the lower Liangshan Formation. The reddened interval near the basal Liangshan Formation of the Xiuhe section was interpreted as having formed during a period of drier climate, which led to better drainage of the alluvial landscape. The reddening, which appeared to be predominantly primary, rather than diagenetic, and the development of desiccation cracks and the pedogenic fabrics all suggested that the water table was lowered some distance below the ground surface for a significant time (e.g., Fielding and Frank, 2015). Wedge-shaped peds, carbonate nodules of different sizes, and coalesced nodule beds formed within the red mudrock matrix. These characters indicated a polygenic paleosol, described as vertic calcisol (Mack et al., 1993). The mottled mudrocks overlying the flood channel coarse-medium sandstones also showed pedogenic characters with mottled horizons, suggesting waterlogging conditions during periodic water table rise. This paleosol was described as gleyed calcic vertisol (Mack et al., 1993). The associated reddish flood coarse sandstones were rich in the silty matrix. They contain high contents of mudrock and siltstone fragments, sometimes in stretched shapes, in addition to subangular, poorly sorted quartzes. Such petrographic characters along with the tabular geometry indicate a rapid deposition and short-distance transportation from proximal sources. The occasional occurrences of carbonate fragments and ooid-like lithic fragments are consistent with this interpretation. Considering the erosional contact of the coarse flood sandstones with the coastal plain paleosols, these fragments are likely derived from the previously formed paleosols with carbonate nodules and ooid-like concretions (Mujal et al., 2018). The gray mudrocks above or below crevasse channel sandstones showed gleysol characters with irregular patches of brown or red in a gray matrix, indicative of pedogenic alteration in a consistently low redox condition (Mack et al., 1993). The associated crevasse channel sandstones showed lateral accretion features with a distinct erosional base and a lenticular geometry. Their model compositions were dominated by well-sorted, subrounded quartz grains. These characters likely indicate relatively long-distance transportation from a distal source by a large fluvial system (Fieldman et al., 2005; Fielding and Frank, 2015).

This stratigraphic upward transition from a thick, high-chroma paleosol to a thinner, low-chroma paleosol in the lower Xiuhe section could indicate more poorly drained conditions (e.g., Fieldman et al., 2005; Mack et al., 1993; Mujal et al., 2018; Miller et al., 1996). Such changes in the pedogenic drainage would indicate rising water tables relative to the ground surfaces and can be ascribed to sea-level rising, climate humidity, or both two (e.g., Fieldman et al., 2005; Miller et al., 1996; Joeckel, 1995). Although successions of the Liangshan Formation were considered to form during an overall transgressive event (e.g., Shen et al., 2019), which tends to raise water tables in the coastal landscapes, relative sea-level variation is complex with multiple rise and fall fluctuations (Wu et al., 2016) and cannot directly be applied to the coastal alluvial plain environments. On the other hand, an arid–semiarid climate is indicated by the pedogenic carbonate nodules and calcic paleosol characters and subsequently changed to more humid or wet conditions as suggested by the low-chroma paleosols without pedogenic carbonate and mire deposition (**Figures 3B,E,F**). A relatively

dry climate for the lower part of the CAP interval is consistent with the rapid deposition of flood-induced weakly confined channel sandstones, which contain abundant locally derived detritus and indicate that only small local drainage networks developed over the shelf (Fieldman et al., 2005). Also for the upper part of the CAP interval, a more humid or relatively wet climate was supported by the well-confined crevasse channel sandstones, which were dominated by well-sorted quartzes transported by relatively large drainage networks from distal source areas (Cecil et al., 2003; Fieldman et al., 2005). Therefore, a relatively arid to seasonally humid climate shift likely occurred during the deposition of the lower Liangshan Formation (**Figures 8C,D**).

Potential Climate Controls on the Coastal Sedimentary Architecture

Facies analysis of the lower Liangshan Formation of Caohai, Houpo, and Mapojiao sections showed a consistently distinct transition from estuarine to deltaic depositions (**Figure 2**). Both deltaic and estuarine sandstones are well-sorted and quartzose. The associated mudrocks are dominated by clay minerals and quartz in mineral composition. These petrological and geochemical characteristics suggested high textural and compositional maturities for these sediments and denoted effective hydraulic sorting and possibly long-term sedimentary recycling. It was noted that the estuarine mudrocks tend to have much higher Al_2O_3/TiO_2 ratios than the deltaic mudrocks (**Figure 7C**). Different Al_2O_3/TiO_2 ratios might suggest different source rocks as both Al and Ti are immobile elements during chemical weathering and can be used to track sedimentary provenance (e.g., Young and Nesbitt, 1998; Yang et al., 2012). Considering the stable tectonic background and rapid facies transition, the higher Al_2O_3/TiO_2 ratios of estuarine mudrocks might plausibly result from the enrichment of marine-derived Al-bearing clay materials relative to the deltaic mudrocks, which are primarily of fluvial origin, supporting the facies interpretation. It is interesting to note that both this estuarine-to-deltaic facies transition and the relatively dry-to-wet climate shift occurred during the deposition of the lower Liangshan Formation. Despite the poor age constraints on these two events, they can be temporally correlated in terms of regional stratigraphic correlations (GZBGMR, 1987; Liu and Xu, 1994) and probably have a genetic linkage.

The coastal sedimentations were largely controlled by sediment supply and sea-level variation, which determine the shoreline migration. Estuaries are common transgressive depositional systems developed when the rise in sea level overtakes the sediment supply (Boyd et al., 1992). The development of estuarine facies at the bottom of the Liangshan Formation, as recorded in the Caohai, Houpo, and Mapojiao sections, supports the view that the Liang Formation represents an overall transgressive sequence (e.g., Shen et al., 2019). The evolution from estuarine to the deltaic environment can be determined by the sediment supply and relative sea-level variation (Boyd et al., 1992; **Figure 8A**). Deltaic sequences of the Holocene age began to accumulate within a restricted time range (Stanley and Warne, 1994), from 8,500–6500 BP (before present), and are generally underlain by estuaries, especially in the river mouth depositional systems of Changjiang, Song Hong, and the Kiso River (Hori and Saito, 2007). These estuarine depositions have been ascribed to the early Holocene rapid deglacial sea-level rise (Hori and Saito, 2007). The subsequent deltaic progradations likely initiated as the rate of fluvial sediment input overtook the sea-level rise along the coasts (Stanley and Warne, 1994). Following the calculations of Hori and Saito (2007), the delta initiation was associated with accelerated sediment accumulation, suggesting the enhancement of sediment supply. For the Ganges and the Brahmaputra River, however, their initial delta growth began 2000–3000 years earlier than the global average because of immense sediment discharge (Goodbred and Kuehl, 2000). With sufficient sediment supply, it maintained relative shoreline stability on the coasts of the Ganges and the Brahmaputra River during the early Holocene rapid sea-level rise. However, during the current sea-level rise, the Mississippi Delta was inevitably drowning because of insufficient sediment supply, as demonstrated by Blum and Roberts (2009). From this point of view, a large sediment supply is critical to promoting delta progradation during a sea-level rise (e.g., Blum and Roberts, 2009). For the Pennsylvanian to early Permian period, it has been proposed that tropical coastal successions are genetically related to climate changes in addition to the eustatic sea level (e.g., Cecil, 1990; Miller et al., 1996; Fieldman et al., 2005). Especially, the deposition of siliciclastic intervals was interpreted as resulting from seasonally humid climate conditions, which tend to promote fluvial transportation (e.g., Allen et al., 2011). According to the studied successions of the lower Liangshan Formation, the estuarine to deltaic transition is characterized by an increase in sandstone proportion and possibly an increase in the sediment accumulation rate. Therefore, this increased sediment supply could be likely related to the enlarged fluvial networks in a more seasonally humid climate relative to the subarid conditions, which tend to limit sediment supply for the estuarine deposition period.

CONCLUSION

Four successions of the late Artinskian Liangshan Formation were studied in Xiuhe, Caohai, Houpo, and Mapojiao sections in western South China. Three facies associations were recognized and are corresponding to coastal alluvial plain, estuarine, and deltaic environments, respectively. The lower Liangshan Formation of the Xiuhe section was interpreted to be deposited in coastal alluvial plain facies association. Paleosols changed stratigraphically upward from calcic to gleyed morphologies throughout this interval. Associated channel sandstones changed from poorly sorted, coarse-grained lithic–quartzose sandstones to relatively well-sorted, fine-/medium-grained quartzose sandstones. Sandstone petrography and paleosol morphology suggest a relatively dry-to-wet climate shift during the deposition of the lower Liangshan Formation. In the lower Liangshan Formation of Mapojiao, Houpo, and Caohai sections, there archived estuarine and overlying deltaic

successions. Sandstone bodies of both these two facies associations were highly quartzose and displayed high textural and compositional maturities, denoting effective hydraulic sorting and extremely weathered source landscapes. Estuarine mudrocks had relatively higher Al_2O_3/TiO_2 ratios than those of deltaic facies, indicating important incorporation of marine clay materials. The estuaries were formed corresponding to the rapid transgression related to the late Artinskian deglaciation and contained marine-derived clay materials with insufficient fluvial sediment supply. The deficiency in sediment supply likely resulted from the arid climate and associated locally small fluvial networks in the coastal plain. The subsequent initiation of deltaic deposition can be primarily interpreted in terms of increased sediment supply, which is sufficient to undertake the sea-level rise-induced accommodation. The increase in sediment supply could be promoted by the climate shift to relatively humid conditions with expanded fluvial systems. This climate control on the coastal sedimentary architecture can be tested in the future by high-resolution stratigraphic correlation and high-precision dating works.

DATA AVAILABILITY STATEMENT

The original contributions presented in the study are included in the article/**Supplementary Material**, further inquiries can be directed to the corresponding author.

AUTHOR CONTRIBUTIONS

AL: investigation and writing—original draft, review, and editing. JY: conceptualization, funding acquisition, project administration, resources, and writing—original draft, review, and editing. LC: investigation. JR: investigation.

FUNDING

This study was financially supported by the National Natural Science Foundation of China (Nos. 41872106 and 42122015).

ACKNOWLEDGMENTS

The authors thank Jishun Yu for help with XRD analysis and Lanlan Jin for help with ICP-MS analysis, and two reviewers for their constructive comments which improved the manuscript.

SUPPLEMENTARY MATERIAL

The Supplementary Material for this article can be found online at: https://www.frontiersin.org/articles/10.3389/feart.2022.888012/full#supplementary-material

REFERENCES

Allen, J. P., Fielding, C. R., Gibling, M. R., and Rygel, M. C. (2011). Fluvial Response to Paleo-Equatorial Climate Fluctuations during the Late Paleozoic Ice Age. *GSA Bull.* 123 (7-8), 1524–1538. doi:10.1130/b30314.1

Belt, E. S., Heckel, P. H., Lentz, L. J., Bragonier, W. A., and Lyons, T. W. (2011). Record of Glacial–Eustatic Sea-Level Fluctuations in Complex Middle to Late Pennsylvanian Facies in the Northern Appalachian Basin and Relation to Similar Events in the Midcontinent Basin. *Sediment. Geol.* 238 (1-2), 79–100. doi:10.1016/j.sedgeo.2011.04.004

Blum, M. D., and Roberts, H. H. (2009). Drowning of the Mississippi Delta Due to Insufficient Sediment Supply and Global Sea-Level Rise. *Nat. Geosci.* 2, 488–491. doi:10.1038/ngeo553

Boyd, R., Dalrymple, R., and Zaitlin, B. A. (1992). Classification of Clastic Coastal Depositional Environments. *Sediment. Geol.* 80 (3-4), 139–150. doi:10.1016/0037-0738(92)90037-r

Buggisch, W., Wang, X., Alekseev, A. S., and Joachimski, M. M. (2011). Carboniferous–Permian Carbon Isotope Stratigraphy of Successions from China (Yangtze Platform), USA (Kansas) and Russia (Moscow Basin and Urals). *Palaeogeogr. Palaeoclimatol. Palaeoecol.* 301 (1-4), 18–38. doi:10.1016/j.palaeo.2010.12.015

Campi, M. J., and Shi, G. R. (2007). TheLinshuichonetes - CrurithyrisCommunity and New Productid Species from the Cisuralian (Early Permian) of Sichuan, China. *Alcheringa Australas. J. Palaeontol.* 31 (2), 185–198. doi:10.1080/03115510701305165

Cecil, C. B., Dulong, F. T., West, R. R., Stamm, R., Wardlaw, B., and Edgar, N. T. (2003). *Climate Controls on the Stratigraphy of a Middle Pennsylvanian Cyclothem in North America*. Broken Arrow, USA: Special Publication, 151–180. doi:10.2110/pec.03.77.0151

Cecil, C. B. (1990). Paleoclimate Controls on Stratigraphic Repetition of Chemical and Siliciclastic Rocks. *Geol* 18 (6), 533–536. doi:10.1130/0091-7613(1990)018<0533:pcosro>2.3.co;2

Crowell, J. C. (1999). Pre-Mesozoic Ice Ages: Their Bearing on Understanding the Climate System. *Geol. Soc. Am.* 81 (47), 570. doi:10.1130/0-8137-1192-4.1

Dickinson, W. R. (1970). Interpreting Detrital Modes of Graywacke and Arkose. *J. Sediment. Res.* 40 (2), 695–707. doi:10.1306/74d72018-2b21-11d7-8648000102c1865d

Dolby, G., Falcon-Lang, H. J., and Gibling, M. R. (2011). A Conifer-Dominated Palynological Assemblage from Pennsylvanian (Late Moscovian) Alluvial Drylands in Atlantic Canada: Implications for the Vegetation of Tropical Lowlands during Glacial Phases. *J. Geol. Soc.* 168 (2), 571–584. doi:10.1144/0016-76492010-061

Eros, J. M., Montañez, I. P., Osleger, D. A., Davydov, V. I., Nemyrovska, T. I., Poletaev, V. I., et al. (2012). Sequence Stratigraphy and Onlap History of the Donets Basin, Ukraine: Insight into Carboniferous Icehouse Dynamics. *Palaeogeogr. Palaeoclimatol. Palaeoecol.* 313-314, 1–25. doi:10.1016/j.palaeo.2011.08.019

Falcon-Lang, H. J. (2004). Pennsylvanian Tropical Rain Forests Responded to Glacial-Interglacial Rhythms. *Geol* 32 (8), 689–692. doi:10.1130/g20523.1

Fielding, C. R., Frank, T. D., Birgenheier, L. P., Rygel, M. C., Jones, A. T., and Roberts, J. (2008). Stratigraphic Imprint of the Late Palaeozoic Ice Age in Eastern Australia: a Record of Alternating Glacial and Nonglacial Climate Regime. *J. Geol. Soc.* 165, 129–140. doi:10.1144/0016-76492007-036

Fielding, C. R., and Frank, T. D. (2015). Onset of the Glacioeustatic Signal Recording Late Palaeozoic Gondwanan Ice Growth: New Data from Palaeotropical East Fife, Scotland. *Palaeogeogr. Palaeoclimatol. Palaeoecol.* 426, 121–138. doi:10.1016/j.palaeo.2015.03.002

Fielding, C. R. (2021). Late Palaeozoic Cyclothems - A Review of Their Stratigraphy and Sedimentology. *Earth-Science Rev.* 217, 103612. doi:10.1016/j.earscirev.2021.103612

Fielding, C. R., Nelson, W. J., and Elrick, S. D. (2020). Sequence Stratigraphy of the Late Desmoinesian to Early Missourian (Pennsylvanian) Succession of Southern Illinois: Insights into Controls on Stratal Architecture in an Icehouse Period of Earth History. *J. Sediment. Res.* 90 (2), 200–227. doi:10.2110/jsr.2020.10

Fieldman, H. R., Franseen, E. K., Joeckel, R. B., and Heckel, P. H. (2005). Impact of Longer-Term Modest Climate Shifts on Architecture of High-Frequency Sequences (Cyclothems), Pennsylvanian of Midcontinent USA. *J. Sediment. Res.* 75 (3), 350–368. doi:10.2110/jsr.2005.028

Garzanti, E. (2016). From Static to Dynamic Provenance Analysis-Sedimentary Petrology Upgraded. *Sediment. Geol.* 336, 3–13. doi:10.1016/j.sedgeo.2015.07.010

Garzanti, E. (2019). Petrographic Classification of Sand and Sandstone. *Earth-Science Rev.* 192, 545–563. doi:10.1016/j.earscirev.2018.12.014

Goodbred, S. L., Jr., and Kuehl, S. A. (2000). The Significance of Large Sediment Supply, Active Tectonism, and Eustasy on Margin Sequence Development: Late Quaternary Stratigraphy and Evolution of the Ganges-Brahmaputra Delta. *Sediment. Geol.* 133, 227–248. doi:10.1016/s0037-0738(00)00041-5

GZBGMR (Guizhou Bureau of Geology and Mineral Resources) (1987). *Regional Geology of Guizhou Province*. Beijing: Geological Publishing House, 1–704. (in Chinese with English abstract).

Heckel, P. H. (1986). Sea-level Curve for Pennsylvanian Eustatic Marine Transgressive-Regressive Depositional Cycles along Midcontinent Outcrop Belt, North America. *Geology* 14 (4), 330–334. doi:10.1130/0091-7613(1986)14<330:SCFPEM>2.0.CO;2

Hori, K., and Saito, Y. (2007). An Early Holocene Sea-Level Jump and Delta Initiation. *Geophys. Res. Lett.* 34 (18), L18401. doi:10.1029/2007gl031029

Huang, X., Aretz, M., Zhang, X., Du, Y., Qie, W., Wen, Q., et al. (2018). Pennsylvanian-earlyPermian Palaeokarst Development on the Yangtze Platform, South China, and Implications for the Regional Sea-Level History. *Geol. J.* 53 (4), 1241–1262. doi:10.1002/gj.2954

Ingersoll, R. V., Bullard, T. F., Ford, R. L., Grimm, J. P., Pickle, J. D., and Sares, S. W. (1984). The Effect of Grain Size on Detrital Modes: a Test of the Gazzi-Dickinson Point-Counting Method. *J. Sediment. Res.* 54 (1), 103–116. doi:10.1306/212f83b9-2b24-11d7-8648000102c1865d

Isbell, J. L., Miller, M. F., Wolfe, K. L., and Lenaker, P. A. (2003). Timing of Late Paleozoic Glaciation in Gondwana: Was Glaciation Responsible for the Development of Northern Hemisphere Cyclothems? *Special Pap. Geol. Soc. Am.* 370, 5–24. doi:10.1130/0-8137-2370-1.5

Jin, Y. G., and Fang, R. S. (1985). Early Permian Brachiopods from the Kuangshan Formation in Luliang County, Yunnan with Notes on Paleogeography of South China during the Liangshanian Stage. *Acta Palaeontol. Sin.* 24 (2), 216–228. (in Chinese with English abstract).

Joeckel, R. M. (1995). Tectonic and Paleoclimatic Significance of a Prominent Upper Pennsylvanian (Virgilian/Stephanian) Weathering Profile, Iowa and Nebraska, USA. *Palaeogeogr. Palaeoclimatol. Palaeoecol.* 118 (3–4), 159–179. doi:10.1016/0031-0182(95)00005-8

Li, X. H., Li, W. X., Li, Z. X., Lo, C. H., Wang, J., Ye, M. F., et al. (2009). Amalgamation between the Yangtze and Cathaysia Blocks in South China: Constraints from SHRIMP U-Pb Zircon Ages, Geochemistry and Nd-Hf Isotopes of the Shuangxiwu Volcanic Rocks. *Precambrian Res.* 174 (1-2), 117–128. doi:10.1016/j.precamres.2009.07.004

Li, Z.-X., Li, X.-h., Zhou, H., and Kinny, P. D. (2002). Grenvillian Continental Collision in South China: New SHRIMP U-Pb Zircon Results and Implications for the Configuration of Rodinia. *Geol* 30 (2), 163–166. doi:10.1130/0091-7613(2002)030<0163:gccisc>2.0.co;2

Liu, B. J., and Xu, X. S. (1994). *Lithofacies Palaeogeography Atlas of South China (Sinian-Triassic Period)*. Beijing: Science Press, 1–188. (in Chinese with English abstract).

Liu, K., Zhang, J., Wilde, S. A., Zhou, J., Wang, M., Ge, M., et al. (2017). Initial Subduction of the Paleo-Pacific Oceanic Plate in NE China: Constraints from Whole-Rock Geochemistry and Zircon U-Pb and Lu-Hf Isotopes of the Khanka Lake Granitoids. *Lithos* 274-275, 254–270. doi:10.1016/j.lithos.2016.12.022

Lv, T. C. (1982). Early Permian Brachiopods from Gaoqiao, Mianchu, Sichuan Province. *Acta Palaeontol. Sin.* 21 (5), 607–612. (in Chinese with English abstract).

Mack, G. H., James, W. C., and Monger, H. C. (1993). Classification of Paleosols. *Geol. Soc. Am. Bull.* 105 (2), 129–136. doi:10.1130/0016-7606(1993)105<0129:cop>2.3.co;2

Martinius, A. W., and Gowland, S. (2011). Tide-influenced Fluvial Bedforms and Tidal Bore Deposits (Late Jurassic Lourinhã Formation, Lusitanian Basin, Western Portugal). *Sedimentology* 58 (1), 285–324. doi:10.1111/j.1365-3091.2010.01185.x

Meng, Q. R. (2017). Origin of the Qinling Mountains (In Chinese). *Sci. Sin. Terrae* 47, 412–420.

Miller, K. B., McCahon, T. J., and West, R. R. (1996). Lower Permian (Wolfcampian) Paleosol-Bearing Cycles of the U.S. Midcontinent: Evidence of Climatic Cyclicity. *J. Sediment. Res.* 66 (1), 71–84. doi:10.1306/d42682b6-2b26-11d7-8648000102c1865d

Montañez, I. P., and Poulsen, C. J. (2013). The Late Paleozoic Ice Age: an Evolving Paradigm. *Annu. Rev. Earth Planet. Sci.* 41, 629–656. doi:10.1146/annurev.earth.031208.100118

Mujal, E., Fortuny, J., Marmi, J., Dinarès-Turell, J., Bolet, A., and Oms, O. (2018). Aridification across the Carboniferous-Permian Transition in Central Equatorial Pangea: The Catalan Pyrenean Succession (NE Iberian Peninsula). *Sediment. Geol.* 363, 48–68. doi:10.1016/j.sedgeo.2017.11.005

Nio, S. D., and Yang, C. S. (1991). "Diagnostic Attributes of Clastic Tidal Deposits: a Review," in *Clastic Tidal Sedimentology*. Editors D. G. Smith, G. E. Reinson, B. A. Zaitlin, and R. A. Rahmani (Calgary, Canada: Canadian Society of Petroleum Geologists, Memoir), 16, 3–28.

Olszewski, T. D., and Patzkowsky, M. E. (2003). From Cyclothems to Sequences: the Record of Eustasy and Climate on an Icehouse Epeiric Platform (Pennsylvanian-Permian, North American Midcontinent). *J. Sediment. Res.* 73 (1), 15–30. doi:10.1306/061002730015

Rosenau, N. A., Tabor, N. J., Elrick, S. D., and Nelson, W. J. (2013). Polygenetic History of Paleosols in Middle-Upper Pennsylvanian Cyclothems of the Illinois Basin, U.S.A.: Part I. Characterization of Paleosol Types and Interpretation of Pedogenic Processes. *J. Sediment. Res.* 83 (8), 606–636. doi:10.2110/jsr.2013.50

Ross, C. A., and Ross, J. R. P. (1985). Late Paleozoic Depositional Sequences Are Synchronous and Worldwide. *Geol* 13 (3), 194–197. doi:10.1130/0091-7613(1985)13<194:lpdsas>2.0.co;2

Rygel, M. C., Fielding, C. R., Frank, T. D., and Birgenheier, L. P. (2008). The Magnitude of Late Paleozoic Glacioeustatic Fluctuations: a Synthesis. *J. Sediment. Res.* 78 (8), 500–511. doi:10.2110/jsr.2008.058

Shen, S., Zhang, H., Zhang, Y., Yuan, D., Chen, B., He, W., et al. (2019). Permian Integrative Stratigraphy and Timescale of China. *Sci. China Earth Sci.* 62 (1), 154–188. doi:10.1007/s11430-017-9228-4

Shi, X., Yu, J., Chen, B., Cheng, H., Hu, i. L., and Chi, H. (2014). Palynology of the Lower Permian Dazhuyuan and Liangshan Formations in Wuchuan-Zheng'an-Daozhen Area, Northern Guizhou Province. *J. Palaeogeogr.* 16 (2), 217–226. (in Chinese with English abstract).

Shu, L. S., Faure, M., Yu, J. H., and Jahn, B. M. (2011). Geochronological and Geochemical Features of the Cathaysia Block (South China): New Evidence for the Neoproterozoic Breakup of Rodinia. *Precambrian Res.* 187 (3-4), 263–276. doi:10.1016/j.precamres.2011.03.003

Smith, L. B., and Read, J. F. (2000). Rapid Onset of Late Paleozoic Glaciation on Gondwana: Evidence from Upper Mississippian Strata of the Midcontinent, United States. *Geology* 28 (3), 279–282. doi:10.1130/0091-7613(2000)28<279:ROOLPG>2.0.CO;2

Stanley, D. J., and Warne, A. G. (1994). Worldwide Initiation of Holocene Marine Deltas by Deceleration of Sea-Level Rise. *Science* 265, 228–231. doi:10.1126/science.265.5169.228

Tabor, N. J., and Poulsen, C. J. (2008). Palaeoclimate across the Late Pennsylvanian–Early Permian Tropical Palaeolatitudes: a Review of Climate Indicators, Their Distribution, and Relation to Palaeophysiographic Climate Factors. *Palaeogeogr. Palaeoclimatol. Palaeoecol.* 268 (3-4), 293–310. doi:10.1016/j.palaeo.2008.03.052

Tandon, S. K., and Gibling, M. R. (1994). Calcrete and Coal in Late Carboniferous Cyclothems of Nova Scotia, Canada: Climate and Sea-Level Changes Linked. *Geol* 22 (8), 755–758. doi:10.1130/0091-7613(1994)022<0755:cacilc>2.3.co;2

Taylor, S. R., and McLennan, S. M. (1985). *The Continental Crust: Its Composition and Evolution*. United States: OSTI.GOV.

Wang, J., and Li, Z. X. (2003). History of Neoproterozoic Rift Basins in South China: Implications for Rodinia Break-Up. *Precambrian Res.* 122 (1-4), 141–158. doi:10.1016/s0301-9268(02)00209-7

Wang, X., Qie, W., Sheng, Q., Qi, Y., Wang, Y., Liao, Z., et al. (2013). Carboniferous and Lower Permian Sedimentological Cycles and Biotic Events of South China. *Geol. Soc. Lond. Spec. Publ.* 376 (1), 33–46. doi:10.1144/sp376.11

Wang, Y., Qian, X., Cawood, P. A., Liu, H., Feng, Q., Zhao, G., et al. (2018). Closure of the East Paleotethyan Ocean and Amalgamation of the Eastern Cimmerian

and Southeast Asia Continental Fragments. *Earth-Science Rev.* 186, 195–230. doi:10.1016/j.earscirev.2017.09.013

Wanless, H. R., and Shepard, F. P. (1936). Sea Level and Climatic Changes Related to Late Paleozoic Cycles. *Geol. Soc. Am. Bull.* 47 (8), 1177–1206. doi:10.1130/gsab-47-1177

Wopfner, H. (2013). Late Palaeozoic-Early Triassic Deposition and Climates between Samfrau and Tethys: A Review. *Geol. Soc. Lond. Spec. Publ.* 376 (376), 5–32. doi:10.1144/sp376.4

Wu, G. Y. (1998). An Introduction to Orogen-Stratigraphy: Taking the Tethysides in the Sanjiang Area, Southwest China as an Example. *J. Stratigr.* 22 (3), 161–181. (in Chinese with English abstract).

Wu, S. Q., Yan, Y. J., Liu, K., and Yan, Y. J. (2016). Response of Early Permian Silisiclastic Depositional System to the Advance of Gondwana Glaciation in Southwestern Guizhou. *Earth Sci. Front.* 23 (6), 299.

Yang, J., Du, Y., Cawood, P. A., and Xu, Y. (2012). Modal and Geochemical Compositions of the Lower Silurian Clastic Rocks in North Qilian, NW China: Implications for Provenance, Chemical Weathering, and Tectonic Setting. *J. Sediment. Res.* 82 (2), 92–103. doi:10.2110/jsr.2012.6

Young, G. M., and Nesbitt, H. W. (1998). Processes Controlling the Distribution of Ti and Al in Weathering Profiles, Siliciclastic Sediments and Sedimentary Rocks. *J. Sediment. Res.* 68 (3), 448–455. doi:10.2110/jsr.68.448

Zhang, R. Y., Lo, C.-H., Chung, S.-L., Grove, M., Omori, s., Iizuka, Y., et al. (2013). Origin and Tectonic Implication of Ophiolite and Eclogite in the Song Ma Suture Zone between the South China and Indochina Blocks. *J. Metamorph. Geol.* 31 (1), 49–62. doi:10.1111/jmg.12012

Zhao, Y. Z., and Huang, J. Q. (1931). *The Geology of the Qinlingshan and Sichuan*. Beijing, China: Geological Survey of China and the Section of Geology of the National Academy of Peiping.

Conflict of Interest: The authors declare that the research was conducted in the absence of any commercial or financial relationships that could be construed as a potential conflict of interest.

Publisher's Note: All claims expressed in this article are solely those of the authors and do not necessarily represent those of their affiliated organizations, or those of the publisher, the editors, and the reviewers. Any product that may be evaluated in this article, or claim that may be made by its manufacturer, is not guaranteed or endorsed by the publisher.